Thermal-hydraulic Analysis in the Pool of PGSFR including the Shielding

Jung Yoon [a*], Tae-ho Lee [a]
[a] *Korea Atomic Energy Research Institute, Fast Reactor Development Div., 1045 Daedeok-daero, Daejeon*
[*] *Corresponding author: jyoon@kaeri.re.kr*

1. Introduction

The thermal-hydraulics of reactor vessel inside is important in the design of a sodium-cooled fast reactor (SFR). Various design issues relate to this region, and one of them is thermal-hydraulic behavior when shielding exists inside the reactor vessel. The shielding is used for the blockage of the radiation emitted by the reactor core. The shielding is installed at the Intermediate Heat eXchanger (IHX), core shroud, and redan region at the top of core[1]. However, this structure disturbs the normal flow path and heat transfer of the primary heat transfer system.

In this study, the multi-dimensional thermal-hydraulic characteristics in the pool of PGSFR including the shielding are analyzed. Also these results are compared to a case in which no shielding is installed[2].

2. Methods and Results

2.1 Geometry and Boundary Condition

The schematic and flow path of a reactor vessel is shown in Fig.1. The reactor vessel inside consists of hot and cold pools which are divided into a redan. The Decay Heat eXchanger (DHX), which carries out the decay heat removal function, is installed at the cold pool. The analysis domain is the whole reactor vessel including the solid component, and the detailed geometry of the reactor vessel inside is shown in Fig.2. The material of the whole solid components except IHX and DHX are SUS316, and the others are Mod9Cr. The core, UIS, IHX, and DHX are defined as a porous media because of the complexity of the geometry and a reduction of the calculation time. Assumptions for the analysis are shown below.

- 3-dimensional, 1/2 symmetry
- Steady-state
- Gravity
- Conjugate heat transfer with solid
- Material properties such as a density, viscosity, specific heat and conductivity are given as a function of temperature
- All walls are no-slip condition except hot and cold pool surface
- Core, UIS, IHX, and DHX: Porous media to satisfy each pressure loss requirements[3]

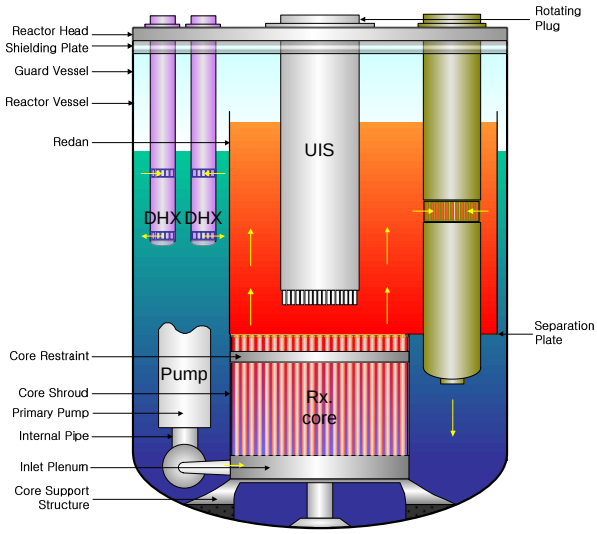

Fig. 1 The schematic and flow path inside a reactor vessel

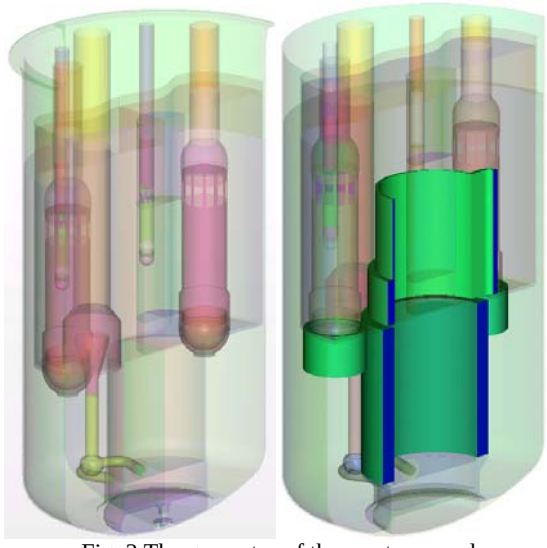

Fig. 2 The geometry of the reactor vessel
(Left : No shielding, Right : Shielding)

All cases are under normal operating conditions. Detailed boundary conditions are shown in Table 1.

Table I: Boundary condition

Case	Inlet		Heat Sink (MWt)		
	Temp. (°C)	Flow Rate (kg/s)	Core	IHX	DHX
Normal Operation	545	994.9	196.1	-98.175	-0.3

2.2 Methodology

A numerical analysis was performed by STAR-CCM+ V8.02.011. A three-dimensional, 1/2 symmetric and steady-state flow is assumed. The conjugate heat transfer through the reactor vessel's internal structure is accounted for. Also, material properties such as the density, viscosity, specific heat and conductivity are given as a function of temperature. Also, the SST $k-\omega$ turbulence model which has an advantage in that it calculates the size of a vortex in the adverse pressure gradient well is used[4] and the total number of computational grids is 9,265,816. The continuity, momentum, energy and SST $k-\omega$ turbulence model equations are shown in Eq. (1) ~ (4).

$$\frac{\partial}{\partial x_i}(\rho u_i) = 0 \tag{1}$$

$$\frac{\partial}{\partial x_i}\left(\rho u_i u_j\right) = -\frac{\partial \mathrm{p}}{\partial x_i} + \frac{\partial}{\partial x_j}\left[\mu\left(\frac{\partial u_i}{\partial x_j}+\frac{\partial u_j}{\partial x_i}-\frac{2}{3}\delta_{ij}\frac{\partial u_i}{\partial x_j}\right)\right] + \frac{\partial}{\partial x_j}\left(-\rho\overline{u_i' u_j'}\right) \tag{2}$$

$$\nabla\cdot\left(\vec{v}(\rho E+p)\right) = \nabla\cdot\left(k_{eff}\nabla \mathrm{T} - \sum_j h_j\overrightarrow{J_J} + \left(\overline{\overline{\tau_{eff}}}\cdot\vec{v}\right)\right) + S_h \tag{3}$$

$$\frac{\partial}{\partial x_i}(\rho u_i k) = \frac{\partial}{\partial x_j}\left(\Gamma_k\frac{\partial k}{\partial x_j}\right) + G_k - Y_k + S_k \tag{4}$$

The pressure loss in a porous media is represented by a viscous and inertial resistance coefficient. Therefore, the pressure loss in a porous media and the loss coefficient k_{loss} are represented by Eq. (5) and (6).

$$\frac{\Delta P}{L} = -(P_v + P_i|v|)v \tag{5}$$

$$k_{loss} = \frac{\Delta P}{\frac{1}{2}\rho v^2} \tag{6}$$

Because a viscous resistance coefficient is the value associated with permeability and its effect is very little in these cases, the inertial resistance coefficient is represented by Eq. (7) in association with Eq. (5) and (6).

$$P_i = \frac{\rho}{2}k_{loss}\frac{1}{L} \tag{7}$$

The loss coefficient is calculated using Eq. (6), and the pressure loss and velocity are obtained by the design value of each component.

2.3 Results

The velocity distributions in IHX, DHX, and the symmetry plane are shown in Fig.3. The shielding structure at the top of the core disturbs the flow toward the IHX inlet. As a result, a flow stagnation region in the lower redan is generated, as shown in Fig.3 (c). Also, the shielding structure at the side of the core shroud disturbs the flow, which starts from the IHX exit rising through the bottom of the reactor vessel. On the other hand, a large vortex structure is generated and mixes the sodium well in the upper and lower redan in a no shielding case because there is no disturbance of the flow in this case.

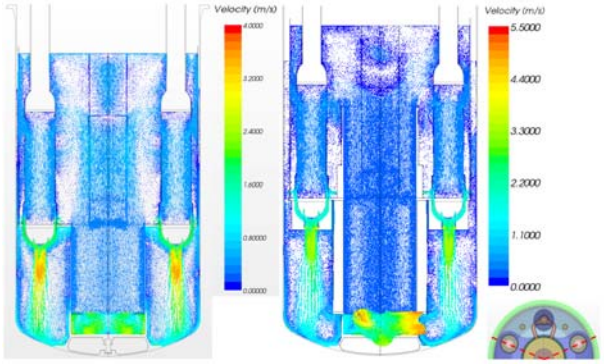

(a) IHX section

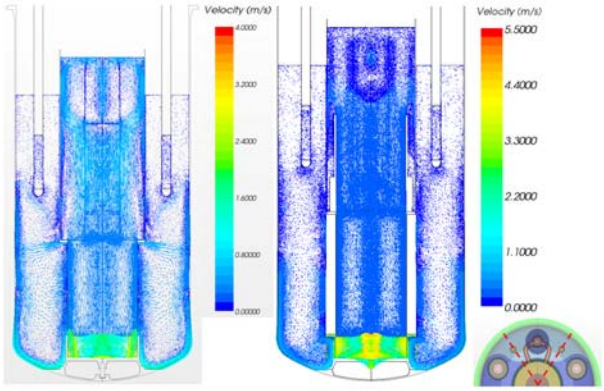

(b) DHX section

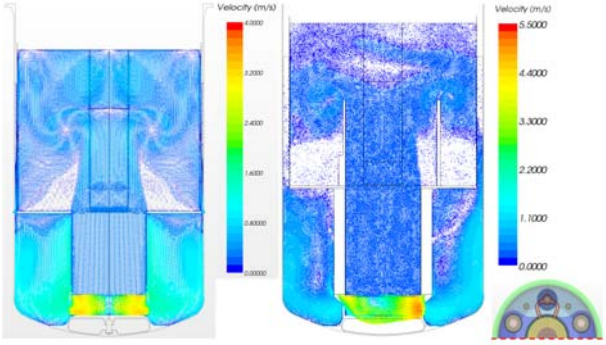

(c) Symmetry section

Fig. 3 Velocity distribution at IHX, DHX, and symmetry section (L: no shielding, R: shielding)

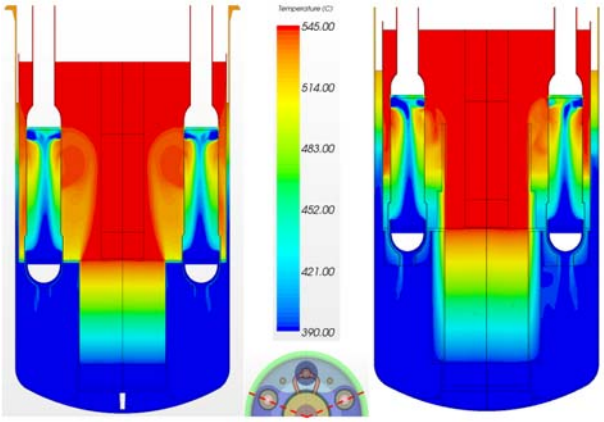

(a) IHX section

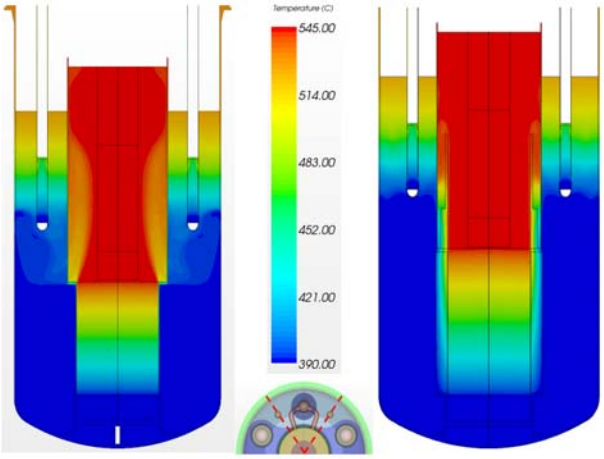

(b) DHX section

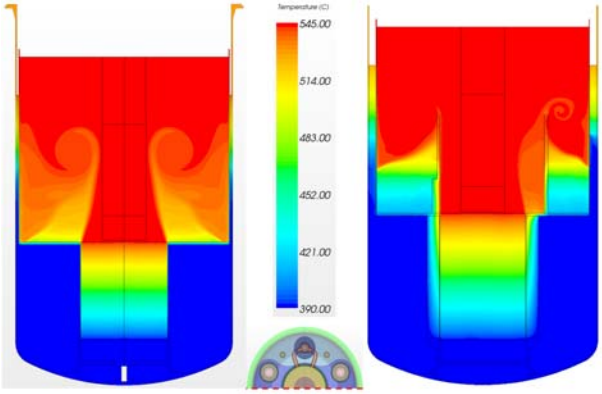

(c) Symmetry section

Fig. 4 Temperature distribution at IHX, DHX, and symmetry section (L: no shielding, R: shielding)

The temperature distributions in IHX, DHX, and the symmetry plane are shown in Fig.4. The heat transfer between the IHX and hot pool is limited by the shielding structure at the top of the core, as shown in Fig.4 (a) and (c). The heat transfer between the hot and cold pools is also limited as shown in Fig.4 (b). However, the overall temperature distribution is substantially similar.

The Z-directional temperature distributions in the hot and cold pools are shown in Fig. 5. Vertical temperature distributions in the hot pool are a little different, as shown in Fig. 5(a). The flow widely spreads in the no shielding case, and thereby hot sodium from the core evenly exists in the hot pool. As a result, the temperature difference between the top and bottom of a hot pool is smaller than that of a shielding case. The vertical temperature distributions at the cold pool between the two cases are almost similar as shown in Fig. 4(b) and Fig. 5(b).

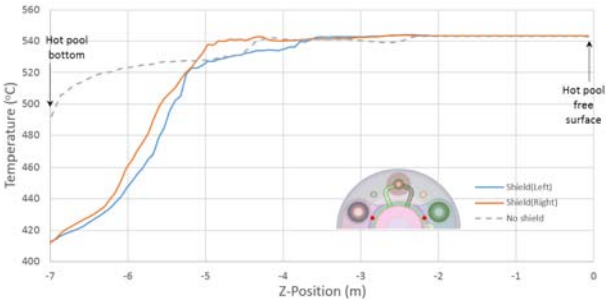

(a) Vertical temperature distribution at a hot pool

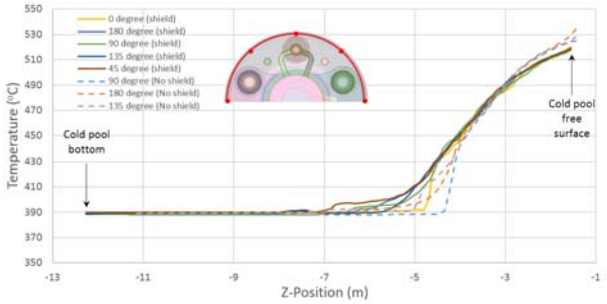

(b) Vertical temperature distribution at a cold pool

Fig. 5 Z-directional line temperature distribution at hot and cold pools

Table II: Mass flow rate (kg/s)

Position	No shield*	Shield	
		Left	Right
IHX in	497.44	497.77	497.12
IHX out	497.45	497.78	497.12
DHX top	2.2225	2.4057	2.4007
DHX bottom	2.2287	2.4002	2.4042

* No shielding case : 1/4 symmetry

Table III: Temperature (°C)

Position	No shield	Shield	
		Left	Right
IHX in	537.02	540.55	538.64
IHX out	391.28	392.03	391.90
ΔT_{IHX}	145.74	148.53	146.74
DHX top	478.70	479.50	479.44
DHX bottom	404.31	408.34	407.75
ΔT_{DHX}	74.39	71.16	71.70
Core inlet	390.18	390.19	
Core outlet	543.13	543.61	
ΔT_{Core}	152.95	153.42	

Table IV: Static Pressure (kPa)

Position	No shield	Shield	
		Left	Right
IHX in	18.77	16.03	16.03
IHX out	2.22	-1.10	-1.08
ΔP_{IHX}	16.55	17.13	17.11
DHX top	0.00	-2.09	-2.09
DHX bottom	0.24	-1.87	-1.87
ΔP_{DHX}	-0.24	-0.22	-0.22
Core inlet	624.38	617.77	
Core outlet	18.69	15.902	
ΔP_{Core}	605.69	601.87	
Inlet Plenum	607.41	613.27	
Inlet	717.76	745.53	
Outlet	-93.56	-89.22	
$\Delta P_{in\text{-}out}$	811.32	834.75	

The flow rate, temperature, and static pressure at a major point are shown in tables II, III, and IV. Although the flow and temperature distributions are slightly different in each case, the physical properties at a major point are almost the same. Thus, the shielding structure does not affect the performance of the primary heat transfer system.

3. Conclusions

A thermal-hydraulic analysis in the pool of the PGSFR considering the shielding structure are performed using STAR-CCM+. The internal major components of the pool inside are modeled, and calculations are performed with a normal operation condition. Also, these results are compared to a no shielding case. The flow and temperature changes owing to the shielding structure at a redan inside are shown, but the overall flow and temperature distributions in both cases are substantially similar. Also the physical properties such as the flow rate, temperature, and static pressure at each major point are almost the same. These results are utilized in the arrangement of the reactor internal structure and design of the shielding structure.

4. Acknowledgement

This work was supported by the National Research Foundation of Korea (NRF) grant funded by the Korean government (MSIP). (No. 2012M2A8A2025624)

REFERENCES

[1] J.H. Cho, PHTS Arrangement and Dimension considering the Core Shielding Structure, KAERI, 2014.
[2] J. Yoon, Thermal-hydraulic Analysis Report for the PGSFR Reactor Vessel inside, KAERI, 2014.
[3] J.H. Cho, Porosity of the IHX, DHX, and UIS for the Thermal-hydraulic Analysis in the PHTS Pool inside, KAERI, 2013.
[4] STAR-CCM+ 8.02.011 User Guide, CD-adapco, 2013.